RSC Advances

PAPER

View Article Online
View Journal | View Issue

Cite this: *RSC Adv.*, 2026, **16**, 13812

Manganese(I) based NN∩SS bis-chelated homo-binuclear metallacycles: synthesis, spectral, crystallographic, anticancer potential and molecular docking studies

Devangana Das, [a] Nivas Saravanan, [a] Abhishek Kumar,[b] Shobhana Krishnaswamy,[c] Arunkumar Dhayalan*[b] and Bala. Manimaran *[a]

Reaction of $Mn_2(CO)_{10}$, dithiooxamide ligand [H_2L = *N*,*N*′-dibutyldithioxamide (dbdto) and *N*,*N*′-diphenethyldithioxamide (dpedto)], and flexible bidentate linkers [L′ = 1,2-bis(4-pyridyl)ethane (bpe), 1,3-bis(4-pyridyl)propane (bpp)] produced binuclear metallacyclic compounds [$(CO)_3Mn(\mu\text{-}\eta^4\text{-}L)(\mu\text{-}L')Mn(CO)_3$] (**1–4**) under ambient reaction conditions. Compounds **1–4** were characterized by elemental analysis, FT-IR, UV-Vis, and NMR spectroscopy, and the formation of dinuclear metallacycles **1–4** was confirmed by high-resolution ESI mass spectrometry. The molecular structure of compound **4** was determined by single-crystal X-ray crystallography, revealing a dinuclear horse-stirrup like framework. The anticancer properties of the metallacycles were investigated *in vitro* on two different cancer cell lines, osteosarcoma (MG-63) and breast cancer (MCF-7), and normal cells (HEK-293). Compounds **2** and **4** showed moderate cytotoxicity toward MG-63 and MCF-7 cells, with IC_{50} values of 65.58 ± 1.54 and 151.19 ± 1.66 μg mL^{-1} for compound **2** and 78.58 ± 3.83 and 125.42 ± 10.77 μg mL^{-1} for compound **4**, respectively, while showing lower toxicity toward HEK-293 cells. Furthermore, qualitative *in silico* docking studies of compound **4** were performed with cancer related proteins, epidermal growth factor receptor tyrosine kinase (EGFRK, PDB ID: 1M17) and human matrix metalloproteinase-9 (MMP-9, PDB ID: 1L6J) to explore possible binding interactions.

Received 13th January 2026
Accepted 2nd March 2026

DOI: 10.1039/d6ra00337k

rsc.li/rsc-advances

Introduction

The process of arranging metal precursors and organic ligands in a way that contains the necessary information for recognition has resulted in the creation of a wide variety of two-dimensional and three-dimensional distinct metal based supramolecular structures.[1,2] A wide variety of unique metallacyclic frameworks have been created using self-assembly processes, and they are increasingly being utilized in a diverse range of fields, including chemosensing, molecular devices, and catalysis.[3–6] Lu and co-workers established several NN∩NN and OO∩OO coordinated Re(I)-based binuclear metallacyclic compounds containing flexible ditopic ligands in a one-step process.[7–9] Manganese(I)-based binuclear metallacycles containing a *fac*-$Mn(CO)_3$ core have shown promise as therapeutic agents due to their bio-medicinal applications. These compounds were synthesized using ditopic pyridyl ligands in a one-step fashion, facilitated by NN∩NN and OO∩OO coordination interactions.[10] In our group, we have already explored a dimanganese metallacyclic system defined by *fac*-$Mn(CO)_3$ metal centers connected by a bis-chelating dibutyloxamidato framework *via* asymmetrical ON∩NO coordination.[6] The coordination chemistry of metals and ligands is significantly influenced by the hard and soft nature of both the metal ions and the ligand donor sites.[11–13] This concept is encapsulated in the Hard and Soft Acids and Bases (HSAB) theory, which categorizes metal ions as either hard or soft based on their polarizability and charge density.[14,15] Hard acids, which are small and have high charge density, tend to prefer coordination with hard bases. Conversely, soft acids, which are larger and have lower charge density, favour soft bases.[16–18] This principle can be applied to predict the stability and reactivity of metal–ligand complexes, including binuclear compounds formed with dithiooxamide.[19] In the context of dithiooxamide ligands, the presence of bulky alkyl substituents can further influence the coordination mode. The ligand can coordinate to metals in various modes, such as κ-*N*,*N*′, κ-*S*,*S*′, or κ-*N*,*S*, depending on the specific interactions dictated by the characteristics of metal and the steric and electronic properties of ligand. For instance, the choice of metal can direct the binding preferences and ultimately the structure

[a]*Department of Chemistry, Pondicherry University, Puducherry, 605014, India. E-mail: manimaran.che@pondiuni.ac.in; Tel: +91-413-2654414*

[b]*Department of Biotechnology, Pondicherry University, Puducherry, 605014, India*

[c]*Sophisticated Analytical Instrument Facility, Indian Institute of Technology-Madras, Chennai, 600036, India*

of the resulting binuclear complex.[20–22] Smaller substituents on the ligand or less crowded coordination environments around the metal center can favor the *cis* configuration. Large or bulky substituents may prefer a *trans* arrangement to minimize steric clashes.[23–25] Lately, sulfur containing chelate ligands like dithiocarbamate compounds have gained attention for their potential as protective agents in cancer treatment. The design of transition-metal-derived therapeutic compounds has recently emerged as a promising strategy for the diagnosis and management of various disorders, ranging from infectious diseases to neurodegenerative conditions and cancer.[26,27] They have been incorporated into gold, palladium, and platinum compounds as anticancer agents, showcasing promising outcomes in studies and the gold compounds as anticancer drugs have shown interesting results.[28] Askari *et al.* have also reported the dithiooxamide chelated Pt and Ru-based heterobimetallic complexes and explored their anticancer activities.[29] Herein, we report the self assembly of thioxamidato bridged Mn(I) homo binuclear metallacycles of the general formula $[(CO)_3Mn(\mu\text{-}\eta^4\text{-}L)(\mu\text{-}L')Mn(CO)_3]$ (**1–4**) synthesized from $Mn_2(CO)_{10}$, dithioxamide, and flexible bispyridyl ligands. The compounds were spectroscopically characterized, with the structure of compound **4** confirmed by single-crystal X-ray diffraction, and their anticancer activity evaluated against MG-63 and MCF-7 cancer cells and normal HEK-293 cells, supported by qualitative molecular docking studies.

Results and discussion

Dithiooxamidato-bridged dinuclear manganese(I) metallacyclic compounds **1–4** were synthesized using dimanganese decacarbonyl, dithiooxamide ligands [H_2L = *N*,*N*′-dibutyldithioxamide (dbdto) and *N*,*N*′-diphenethyldithiooxamide (dpedto)], and flexible bidentate bis pyridyl ligands [L′ = 1,2-bis(4-pyridyl)ethane (bpe) and 1,3-bis(4-pyridyl)propane (bpp)]. Equimolar quantities of $Mn_2(CO)_{10}$, dithiooxamide ligands, and bis pyridyl ligands, along with trimethylamine-*N*-oxide, resulted in the formation of manganese(I)-based metallacyclic compounds **1–4**, with the common formula $[(CO)_3Mn(\mu\text{-}\eta^4\text{-}L)(\mu\text{-}L')Mn(CO)_3]$ (Scheme 1). The compounds were synthesized at ambient reaction conditions and isolated under dark condition due to the light sensitive nature of Mn(I) compounds. Oxidative addition of the dithiooxamide ligands to $Mn_2(CO)_{10}$ led to the formation of the metallacycles by cleaving metal–metal bond and chelating through NN∩SS coordination at the equatorial sites of the *fac*-$Mn(CO)_3$-core. Furthermore, the flexible bis pyridyl bidentate linker coordinated orthogonally at the axial sites. Metallacycles **1–4** are soluble in common polar organic solvents and were characterized using standard spectroscopic techniques. The molecular structure of the 1,3-bis(4-pyridyl) propane containing metallacycle **4** was confirmed by single-crystal X-ray diffraction analysis, and the molecular masses of **1–4** were determined by HR-ESI mass spectrometry.

The FT-IR spectra of compounds **1–4** showed three strong stretching bands in the range ν 2012–1913 cm^{-1} matching to the terminal carbonyl ligands of *fac*-$Mn(CO)_3$-core.[6] The medium bands at ν 2026 and 2025 cm^{-1} indicated the symmetrical *cis* chelation of dithioxamide ligand to the *fac*-$Mn(CO)_3$.[30] Further, a band in the range ν 1493–1498 cm^{-1} was characteristic to the N–C=S stretching frequency band of the bridging dithiooxamide ligand (Fig. S1).[31] The shift of the dithiooxamide N–C=S stretching frequency band and the disappearance of the NH stretching frequency band in comparison with the spectra of free dithiooxamide ligands revealed the chelation of the dithiooxamide ligands between the two metal cores. The UV-Vis absorption spectra of **1–4** in dichloromethane revealed two different intraligand transitions at λ_{max} 232–235 and 301–307 nm, and the MLCT transitions appeared in the region λ_{max} 437–442 nm (Fig. S3).[6] ^{1}H NMR spectra of compounds **1–4** display two resonances at δ 8.41–8.30 and 7.91–7.75 ppm, attributed to the H^2 py protons adjacent to sulfur and nitrogen in the bpe and bpp ligands. The corresponding H^2 py protons appear as two doublets in the region δ 6.86–6.56 ppm. In addition, compounds **2** and **4** exhibit aromatic signals from

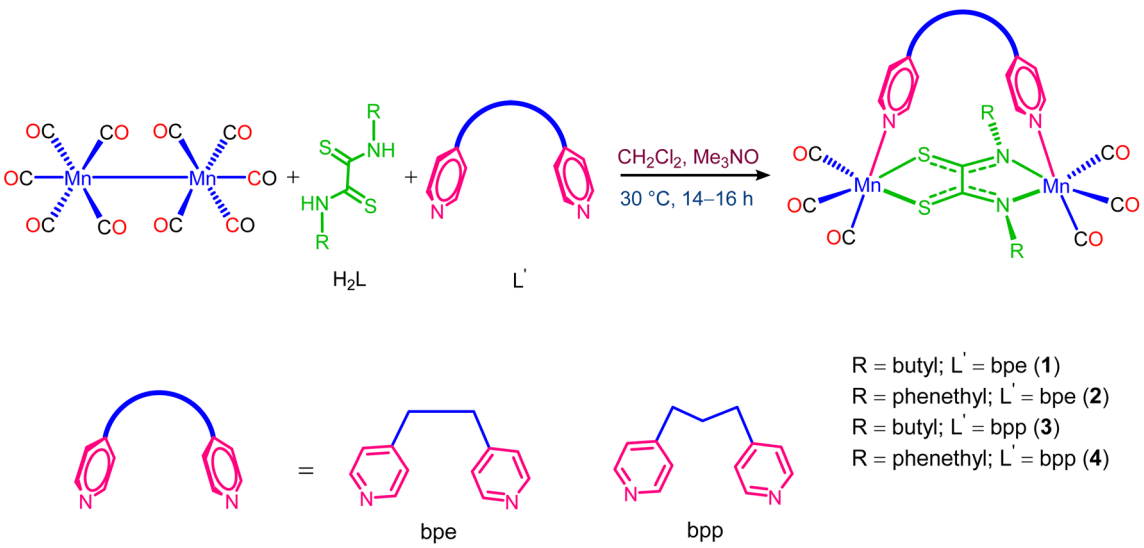

Scheme 1 Self-assembly of dithiooxamidato chelated dimanganese(I) metallacycles **1–4**.

the phenethyl dithiooxamidato bridge as multiplets between δ 7.50 and 7.27 ppm (Fig. S2). The upfield shift of the pyridyl proton signals in **1–4**, along with the disappearance of the dithiooxamide NH resonance relative to the free ligand, confirms ligand coordination to the metal centers.[32,33] The diastereotopic methylene (–CH_2–) protons adjacent to the dithiooxamidato nitrogen appear as doublets at δ 4.85–3.71 ppm,[33,34] while the aliphatic protons of the bpe and bpp ligands and the dibutyldithiooxamidato fragment resonate as multiplets in the regions δ 3.26–2.25 and 1.96–0.95 ppm, respectively. The ^{13}C NMR spectra for complexes **1–4** revealed three resonances ranging from δ 193.2 to 190.8 ppm, which are associated with the three terminal carbonyl ligands of the *fac*-Mn(CO)$_3$-core. The evidence for the formation of dithiooxamidato-bridged compounds **1–4** with bis pyridyl ligands has been obtained using ESI-MS mass spectrometry. The isotopic distribution patterns attained for the molecular-ion peaks related to $[\mathbf{1} + H]^+$, $[\mathbf{2} + H]^+$, $[\mathbf{3} + H]^+$ and $[\mathbf{4} + H]^+$ at m/z = 693.0435, 789.0444, 707.0621 and 803.0618 match the theoretical isotopic distribution patterns for the assembly of binuclear compounds (Fig. S4–S7).

Good quality single-crystals of the Mn(I) based metallacycle **4** interconnected by bis-dithiooxamidato chelate ligand were successfully grown through diffusion of CH_2Cl_2 into a hexane solution of the complex at 5 °C in the absence of light. X-ray diffraction data were recorded for a crystal of **4** at 100 K and the structure was solved and refined. The specifics of the data collection, solution, and refinement are summarised in Table 1. Compound **4**·CH_2Cl_2 crystallized in the monoclinic space group $P2_1/c$. The molecular structure **4** is illustrated in Fig. 1. Selected bond lengths and angles for compound **4** are listed in Table 2. The crystal structure of **4** showed a metallacycle containing two hetero ligand coordinated manganese metal cores, wherein two *fac*-Mn(CO)$_3$ cores are bridged by a bis-(chelating) diphenethyldithiooxamidato group *via* symmetrical NN∩SS chelation mode.[22,30] The manganese cores are moreover connected by a flexible bidentate bpp ligand through manganese Mn–N coordination mode. The diphenethyldithiooxamidato chelate ligand and the capping dipyridyl linkers are oriented in an orthogonal fashion to form the binuclear metallacyclic compound. The structural aspects have a close similarity to a horse stirrup. The octahedral environment around Mn(I) core is comprised of three terminal carbonyl groups, sulfur atoms S(1) and S(2) from the dithiooxamidato group and a nitrogen atom from bpp, while that around the Mn(2) core consists of three terminal carbonyl groups, nitrogen atoms N(3) and N(4) from the dithiooxamidato group, and a nitrogen atom from bpp. The Mn···Mn intracyclic distance in metallacycle **4** is 5.8558(6) Å. The phenethyl substituents on the dithiooxamidato group are located away from the bpp ligand. The centroid–centroid distance between the two pyridyl groups of the bpp

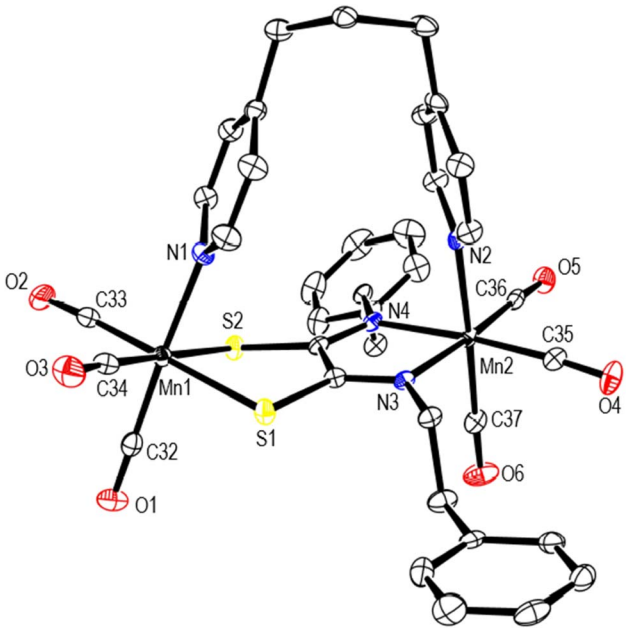

Fig. 1 ORTEP representation of **4** with thermal ellipsoids drawn at the 50% probability level. Hydrogen atoms and solvent molecules are excluded for clarity.

Table 1 Crystallographic data and structure refinement of **4**

Compound	**4**·CH_2Cl_2
Empirical formula	$C_{38}H_{34}Cl_2Mn_2N_4O_6S_2$
Formula weight	887.59
Crystal system	Monoclinic
Temperature [K]	100(2) K
Space group	$P2_1/c$
a [Å]	10.3703(3)
b [Å]	20.9368(7)
c [Å]	18.2449(5)
α [°]	90
β [°]	90.7820(10)
γ [°]	90
Volume [A^3]	3961.0(2)
Z	4
F(000)	1816
D_{calc} [mg m^{-3}]	1.488
μ (mm^{-1})	0.928
h, k, l collected	−13, 13; −26, 26; −23, 22
Theta range for data collection [°]	3.489 to 27.106
Crystal size [mm]	0.215 × 0.139 × 0.055
Reflections collected/unique/R_{int}	82 829/8711/0.0582
Data/restraints/parameters	8711/0/487
Final R indices [$I > 2$ sigma(I)]	$R_1 = 0.0443$, $wR_2 = 0.0960$
Goodness-of-fit on F^2	1.100
R Indices (all data)	$R_1 = 0.0545$, $wR_2 = 0.1003$
Largest diff. peak and hole	0.966 and −0.730 e A^{-3}
CCDC number	2471972

Table 2 Selected bond lengths (Å) and angles (deg) for **4**

Mn(1)–N(1)	2.117(2)	S(1)–Mn(1)–N(1)	87.65(6)
Mn(2)–N(2)	2.107(2)	S(1)–Mn(1)–C(34)	90.88(9)
Mn(1)–S(1)	2.3586(7)	S(2)–Mn(1)–N(1)	88.47(6)
Mn(1)–S(2)	2.3575(7)	N(3)–Mn(2)–C(35)	95.76(9)
Mn(2)–N(3)	2.0397(19)	N(3)–Mn(2)–N(2)	87.94(8)
Mn(2)–N(4)	2.036(2)	N(4)–Mn(2)–N(2)	85.65(8)

ligand is 4.046 Å (Fig. S15a). Two phenethyl groups of the dithiooxamidato panel are oriented *trans* to each other and directed away from bpp ligand (Fig. S15b). The packing diagram of **4**·CH_2Cl_2 along *a* axis displayed CH_2Cl_2 molecules present in between the molecules of compound **4** (Fig. S15c). The packing diagram of **4** along the *c* axis shows zig-zag chain formation (Fig. S16) and the compound **4** showed O(5)…H(13) type hydrogen bonding interaction between the O(5) and pyridine hydrogen H(13) of the nearby metallacycle with a distance of 2.622 Å (Fig. S17).

Cytotoxicity studies of homo-binuclear metallacycles

To determine the cytotoxic effect of compounds **2** and **4**, we performed MTT assay on (i) MG-63 (osteosarcoma cancer cell line), (ii) MCF-7 (breast cancer cell line), and (iii) HEK-293 (normal immortalized cell line) at different concentrations.[35–39] We observed that the compounds exhibited medium-level of cytotoxicity to the MG-63 osteosarcoma and MCF-7 breast cancer cells (Fig. 2, 3 and Table 3) and the cytotoxicity of these compounds are much lower in the normal immortalized HEK-293 cells suggesting that these compounds have the moderate potential for cancer therapy applications (Fig. 4 and Table 3). The compounds **2** and **4** reduced the viability of MG-63 cells and MCF-7 cells by more than 85% at 100 μg mL^{-1} concentration. Cisplatin exhibits significantly higher cytotoxic activity against both MCF-7 (breast cancer), MG-63 (osteosarcoma) and HEK-293 (normal cells) cancer cell lines, with low IC_{50} values of 5.57 ± 1.08 μg mL^{-1}, 3.87 ± 0.3 μg mL^{-1} and 5.29 ± 0.86 μg mL^{-1} respectively.[40–42] However, Compounds **2** and **4** exhibit lower toxicity toward normal cells, which may offer an advantage in reducing side effects, despite lower potency. All these data establish that these compounds hold moderate potential for cancer therapy applications. Additionally, the stability of compounds **2** and **4** in solution was evaluated in 0.1% DMSO/DMEM using a time-dependent UV-Vis absorption spectroscopy, as shown in Fig. S11 and S12. These UV-Vis spectra of **2** and **4** exhibited characteristic absorption bands, consistent with *fac*-$Mn(CO)_3$-core based compounds. A minor decrease in absorbance was observed during the first 24 h, likely due to medium equilibration or minor structural modifications. Thereafter, the spectrum remained unchanged for up to 48 h, with no peak shifts or new bands, indicating the absence of precipitation, aggregation, or degradation.[43] Furthermore, the stability of compound **2** and **4** in DMSO was monitored by UV-Vis spectroscopy and showed no change over 48 h (Fig. S13 and S14).[44] These results suggest that **2** and **4** retains its appreciable stability[45] in under the experimental conditions.

Table 3 Cytotoxic effects of compounds **2** and **4** in cancer and normal cells

	IC_{50} value μg mL^{-1}		
Compound	MG-63	MCF-7	HEK-293
2	65.58 ± 1.54	78.58 ± 3.83	149.83 ± 2.65
4	151.19 ± 1.66	125.42 ± 10.77	196.17 ± 3.18
Cisplatin	3.87 ± 0.3	5.57 ± 1.08	5.29 ± 0.86

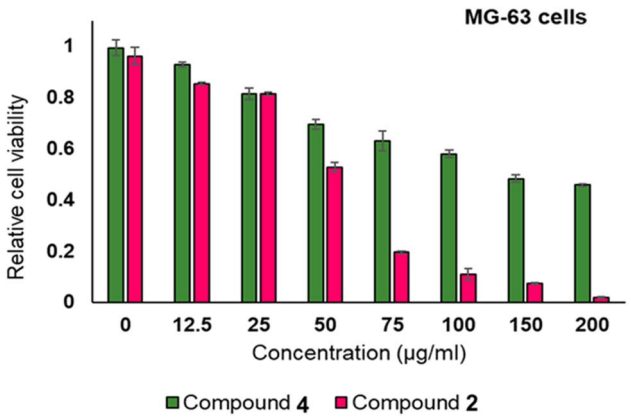

Fig. 2 MTT assay of the compounds **2** and **4** on MG-63 cells to study the cytotoxicity of these compounds.

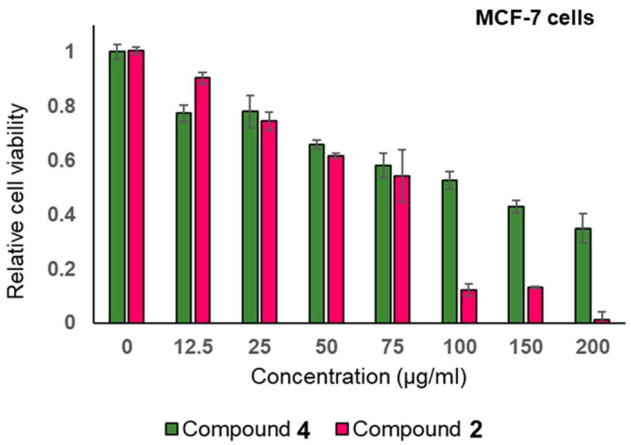

Fig. 3 MTT assay of the compounds **2** and **4** on MCF-7 cells to study the cytotoxicity of these compounds.

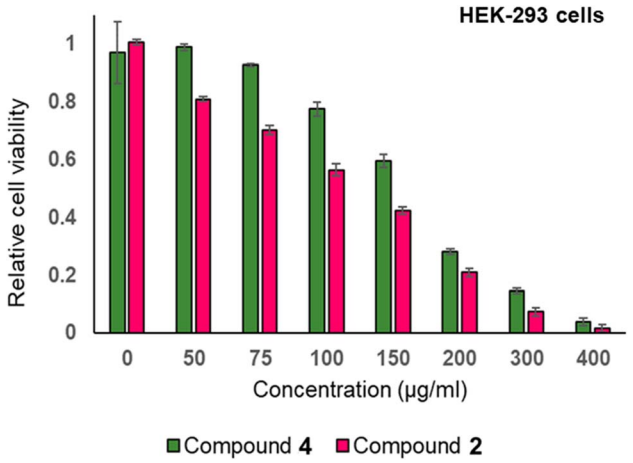

Fig. 4 MTT assay of the compounds **2** and **4** on HEK-293 cells to study the cytotoxicity of these compounds.

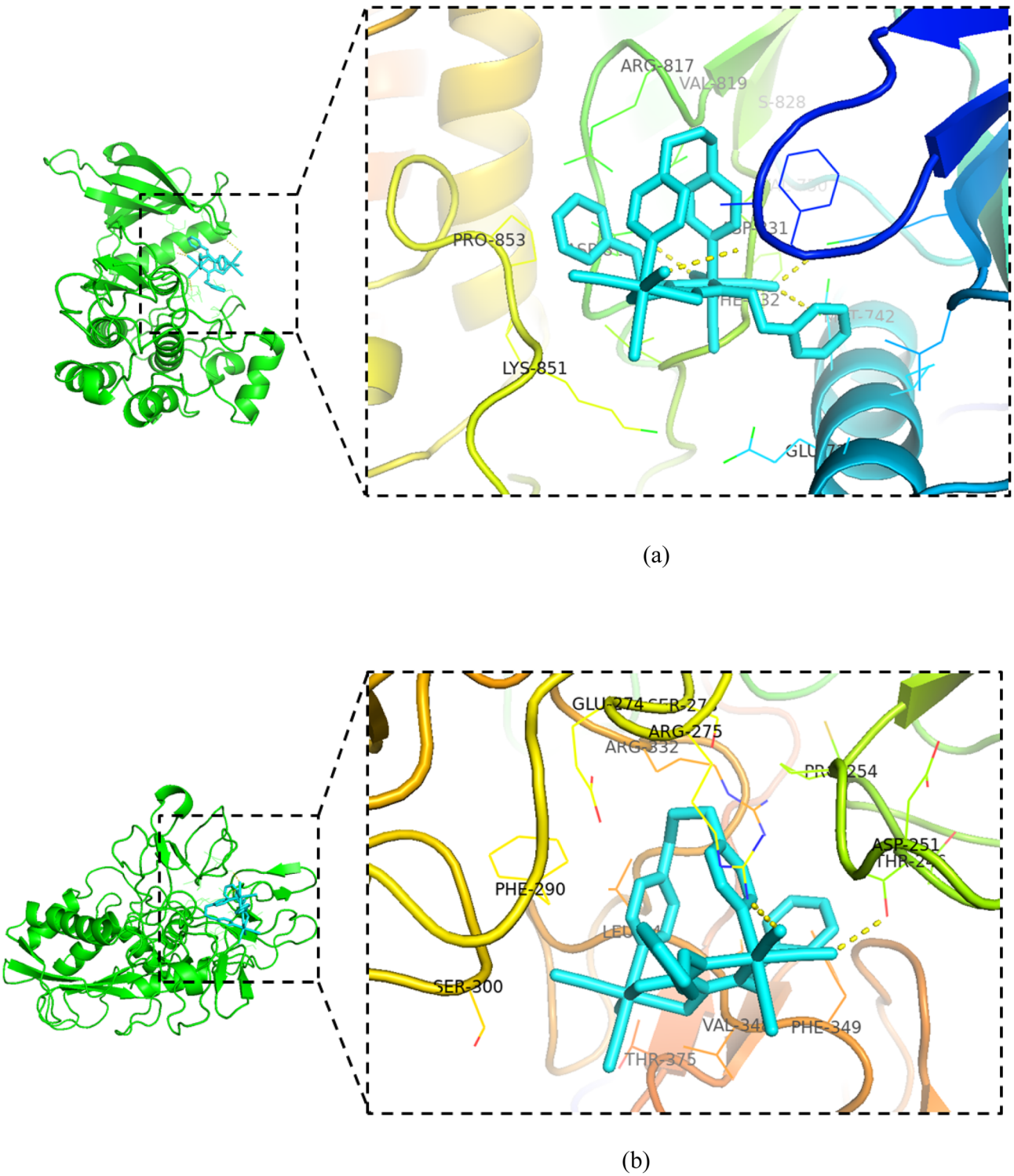

Fig. 5 (a) Plausible interactions of metallacycle **4** against epidermal growth factor receptor tyrosine kinase (PDB ID: 1M17), (b) plausible interactions of metallacycle **4** against human matrix metalloproteinase-9 (PDB ID: 1L6J).

Molecular docking analysis

Molecular docking methods serve as an essential approach in drug discovery, enabling detailed examination of how potential drug candidates interact with their biological targets. These techniques allow researchers to predict the possible biological activities of molecules even before their actual synthesis, offering insights that go beyond conventional experimental activity assessments. Cavity based blind docking studies were carried out to assess the qualitative binding interactions of compound **4** with biologically relevant cancer targets, including epidermal growth factor receptor tyrosine kinase (EGFR, PDB

ID: 1M17),[46] and human matrix metalloproteinase-9 (MMP-9, PDB ID: 1L6J),[47] a well-established cancer based therapeutic targets.[48] The results obtained from the molecular docking for compound **4** are presented in Fig. 5 Based on the cavity detection and AutoDock Vina[49] scoring algorithm integrated in the CB-Dock2 platform, five possible binding models were generated for each protein.[50,51] The vina scores were used to predict the most favorable interactions. Among these, the docking pose with the lowest binding energy was selected in each case, and in the event of identical scores, the model corresponding to the largest active cavity was chosen (Table S1). Accordingly, the EGFRK (1M17) structure exhibited a favorable binding interaction, followed closely by MMP-9 (1L6J). The docking results suggest that compound **4** shows plausible interactions with cancer-associated proteins. The ligand–protein interactions involving amino acid residues for **4** in EGFR (1M17) and MMP-9 (1L6J) are illustrated in Fig. S8–S10.

Conclusion

We have effectively synthesized neutral molecular manganese(I)-based dinuclear metallacycles with a stirrup-like shape using NN∩SS chelation *via* self-assembly process. The self-assembly of three precursors was achieved by introducing dithiooxamide ligands to manganese carbonyl with flexible ditopic linkers, using an orthogonal bonding approach. The compounds were investigated using spectroscopic techniques and the homo-binuclear metallacyclic architecture of **4** was determined by single-crystal X-ray diffraction studies. The anticancer potential of manganese(I) compounds **2** and **4** with flexible pyridyl linkers bridged by dithiooxamidato ligand was examined on two different types of cancer cells and normal cells, and these compounds possess moderate potential for anticancer therapy applications. Molecular docking studies of the compound **4** demonstrated its possible binding interactions toward key biological targets, including epidermal growth factor receptor tyrosine kinase and human matrix metalloproteinase-9, supporting its promise as a bioactive candidate. The ongoing research focuses on the synthesis of manganese(I) compounds with varying geometries, bridged by dithiooxamidato ligands that exhibit potential biological activities.

Experimental section

Instruments and materials

The procedures were conducted in a dry, oxygen-free N_2 environment using standard Schlenk techniques. $Mn_2(CO)_{10}$ was bought from Strem Chemicals, while bpe and bpp were obtained from Sigma-Aldrich. The secondary dithiooxamide ligands were prepared as previously reported.[52] The synthesis, workup, isolation and crystallization of the manganese metallacyclic compounds were carried out in the absence of light. Dichloromethane and other solvents were purified using standard procedures and freshly distilled before use.[53] All metallacyclic compounds were meticulously dried in a high-vacuum conditions for several hours before spectroscopic studies. FT-IR spectra were recorded using a Thermo Nicolet 6700 FT-IR spectrometer. Absorption spectra were collected using a Shimadzu UV-2450 spectrophotometer. Elemental composition was determined with a Thermo Scientific Flash 2000 CHNS analyzer. ^{1}H NMR spectra were obtained with a Bruker Avance 400 MHz spectrometer, and the HR-ESI mass spectra were recorded by using an Agilent 6530B Accurate-Mass Q-TOF LC/MS mass spectrometer.

Synthesis of $[(CO)_3Mn(\mu\text{-}\eta^4\text{-dbdto})(\mu\text{-bpe})Mn(CO)_3]$ (1)

A combination of $Mn_2(CO)_{10}$ (39 mg, 0.1 mmol), *N*,*N*′- dibutyldithiooxamide (23 mg, 0.1 mmol), bpe (20 mg, 0.1 mmol), and trimethylamine *N*-oxide (17 mg, 0.2 mmol) were added in two-neck round-bottom flask with a magnetic stirring bar. The setup was evacuated and flushed with nitrogen gas using a Schlenk line. Under a nitrogen atmosphere, freshly distilled dichloromethane (15 mL) was added to the mixture, and the solution was stirred at 30 °C for 16 hours. Color of the reaction mixture changed from yellow to orange. After removing the solvent, the mixture was purified by silica gel column chromatography using a dichloromethane and hexane as an eluent and dried under vacuum. The product was separated as an orange solid. Yield 52 mg, 59% [based on $Mn_2(CO)_{10}$]. Calc. for $C_{28}H_{30}N_4O_6S_2Mn_2$: C, 48.56; H, 4.37; N, 8.09. Found: C, 48.13; H, 4.29; N, 7.97. IR (CH_2Cl_2, cm^{-1}): $\nu_{(CO)}$ 2025 (m), 2012 (vs), 1927 (s), 1912 (s), $\nu_{(\text{aromatic C=C})}$ 1606 (w), $\nu_{(\text{dithiooxamide N–C=S})}$ 1496 (w). ^{1}H NMR (400 MHz, $CDCl_3$): δ 8.41 (s, 2H, H^2, py (nitrogen)), 7.91 (s, 2H, H^2, py (sulfur)), 6.78 (s, 2H, H^3, py (nitrogen)), 6.62 (s, 2H, H^3, py (sulfur)), 4.55 (s, 2H, H^1, CH_2-dithiooxamidato), 3.77 (s, 2H, $H^{1\prime}$, CH_2-dithiooxamidato), 3.14 (s, 2H, CH_2-bpe, sulfur), 2.94 (s, 2H, CH_2-bpe, nitrogen), 1.93 (s, 4H, H^2, CH_2-dithiooxamidato) 1.58 (s, 4H, H^3, CH_2-dithiooxamidato), 0.95 (s, 4H, H^4, CH_2-dithiooxamidato) ppm. ^{13}C NMR (100 MHz, $CDCl_3$): δ = 193.5 (thioamide CS), 192.0, 191.5, 190.8 [$Mn(CO)_3$], 154.9 (C^2, py, nitrogen), 153.4 (C^4, py, nitrogen), 152.1 (C^2, py, sulfur), 151.7 (C^4, py, sulfur), 125.2 (C^3, py, nitrogen), 124.0 (C^3, py, sulfur), 60.4 (C^1, butyl), 34.7 (methylene), 29.6 (C^2, butyl), 20.8 (C^3, butyl), 14.0 (C^4, butyl) ppm. UV-Vis (λ_{max}^{ab} (CH_2Cl_2), nm): 234, 302 (LIG); 439 (MLCT). HRMS (ESI) Calcd for $C_{28}H_{30}N_4O_6S_2Mn_2$, $[M + H]^+$: *m*/*z* 693.0446; found: 693.0435.

Synthesis of $[(CO)_3Mn(\mu\text{-}\eta^4\text{-dpedto})(\mu\text{-bpe})Mn(CO)_3]$ (2)

Compound **2** was attained by following a corresponding procedure as that for **1** with a mixture of $Mn_2(CO)_{10}$ (39 mg, 0.1 mmol), *N*,*N*′-diphenethyldithiooxamide (33 mg, 0.1 mmol), bpe (20 mg, 0.1 mmol), and trimethylamine *N*-oxide (17 mg, 0.2 mmol). The reaction mixture was stirred at 30 °C for 14 h under the atmosphere of nitrogen gas. The product was isolated as an orange solid. Yield 52 mg, 75% (based on $Mn_2(CO)_{10}$). Calc. for $C_{36}H_{30}N_4O_6S_2Mn_2$: C, 54.83; H, 3.83; N, 7.10. Found: C, 54.68; H, 3.94; N, 6.73. IR (CH_2Cl_2, cm^{-1}): $\nu_{(CO)}$ 2026 (m), 2013 (vs), 1928 (s), 1917 (s), $\nu_{(\text{aromatic C=C})}$ 1602 (w), $\nu_{(\text{dithiooxamide N–C=S})}$ 1493 (w). ^{1}H NMR (400 MHz, $CDCl_3$): δ 8.39 (s, 2H, H^2, py (nitrogen)), 7.90 (s, 2H, H^2, py (sulfur)), 7.50 (s, 4H, H^2, Ph), 7.40 (s, 4H, H^3, Ph), 7.30 (s, 2H, H^4, Ph), 6.70 (s, 2H, H^3, py (nitrogen)), 6.56 (s, 2H, H^3, py (sulfur)), 4.74 (s, 2H, H^1, CH_2-

dithiooxamidato), 3.93 (s, 2H, $H^{1\prime}$, CH_2-dithiooxamidato), 3.26 (s, 2H, H^2, CH_2-dithiooxamidato), 3.11 (s, 4H, (2H, $H^{2\prime}$, CH_2-dithiooxamidato and 2H, CH_2-bpe, sulfur), 2.94 (s, 2H, CH_2-bpe, nitrogen), ppm. ^{13}C NMR (100 MHz, $CDCl_3$): δ = 194.4 (thioamide CS), 192.7, 191.5, 190.9 [$Mn(CO)_3$], 155.0 (C^2, py, nitrogen), 153.3 (C^4, py, nitrogen), 152.0 (C^2, py, sulfur), 152.2 (C^4, py, sulfur), 138.9, 128.7, 126.6 (Ph, aromatic), 125.4 (C^3, py, nitrogen), 124.5 (C^3, py, sulfur), 62.6, 33.5 (phenethyl), 33.4 (methylene) ppm. UV-Vis ($\lambda_{max}{}^{ab}$ (CH_2Cl_2), nm): 233, 307 (LIG); 442 (MLCT). HRMS (ESI) Calcd for $C_{36}H_{30}N_4O_6S_2Mn_2$, $[M + H]^+$: m/z 789.0446; found: 789.0444.

Synthesis of $[(CO)_3Mn(\mu\text{-}\eta^4\text{-dbdto})(\mu\text{-bpp})Mn(CO)_3]$ (3)

Compound **3** was attained by following a corresponding procedure as that for **1** with a mixture of $Mn_2(CO)_{10}$ (39 mg, 0.1 mmol), *N*,*N*′- dibutyldithiooxamide (23 mg, 0.1 mmol), bpp (20 mg, 0.1 mmol), and trimethylamine *N*-oxide (17 mg, 0.2 mmol). The reaction mixture was stirred at 30 °C for 15 h under the atmosphere of nitrogen gas. The product was separated as an orange solid, yield 52 mg, 59% [based on $Mn_2(CO)_{10}$]. Calc. for $C_{29}H_{32}N_4O_6S_2Mn_2$: C, 49.30; H, 4.57; N, 7.93. Found: C, 49.20; H, 4.87; N, 7.85. IR (CH_2Cl_2, cm^{-1}): $\nu_{(CO)}$ 2025 (m), 2011 (vs), 1926 (s), 1911 (s), ν $_{(aromatic\ C=C)}$ 1617 (w), ν $_{(dithiooxamide\ N-C=S)}$ 1498 (w). ^1H NMR (400 MHz, $CDCl_3$): δ 8.33 (s, 2H, H^2, py (nitrogen)), 7.79 (s, 2H, H^2, py (sulfur)), 6.86 (s, 2H, H^3, py (nitrogen)), 6.74 (s, 2H, H^3, py (sulfur)), 4.65 (s, 2H, H^1, CH_2-dithiooxamidato), 3.72 (s, 2H, $H^{1\prime}$, CH_2-dithiooxamidato), 2.79 (s, 4H, H^1, CH_2-bpp), 2.29 (s, 2H, H^2, CH_2-bpp), 1.96 (s, 4H, H^2, CH_2-dithiooxamidato) 1.54 (s, 4H, H^3, CH_2-dithiooxamidato), 1.07 (s, 6H, H^4, CH_2-dithiooxamidato) ppm. ^{13}C NMR (100 MHz, $CDCl_3$): δ = 193.5 (thioamide CS), 192.5, 191.5, 190.8 [$Mn(CO)_3$], 154.9 (C^2, py, nitrogen), 152.7 (C^4, py, nitrogen), 151.8 (C^2, py, sulfur), 150.7 (C^4, py, sulfur), 125.6 (C^3, py, nitrogen), 124.2 (C^3, py, sulfur), 60.5 (C^1, butyl), 36.1 (C^2, butyl), 29.7, 27.2 (methylene), 20.93 (C^3, butyl), 14.1 (C^4, butyl) ppm. UV-Vis ($\lambda_{max}{}^{ab}$ (CH_2Cl_2), nm): 235, 301 (LIG); 438 (MLCT). HRMS (ESI) Calcd for $C_{29}H_{32}N_4O_6S_2Mn_2$, $[M + H]^+$: m/z 707.0603; found: 707.0621.

Synthesis of $[(CO)_3Mn(\mu\text{-}\eta^4\text{-dpedto})(\mu\text{-bpp})Mn(CO)_3]$ (4)

Compound **4** was attained by following a corresponding procedure as that for **1** with a mixture of $Mn_2(CO)_{10}$ (39 mg, 0.1 mmol), *N*,*N*′-diphenethyldithiooxamide (33 mg, 0.1 mmol), bpp (20 mg, 0.1 mmol), and trimethylamine *N*-oxide (17 mg, 0.2 mmol). The reaction mixture was stirred at 30 °C for 14 h under the atmosphere of nitrogen gas. The product was separated as an orange solid, yield 52 mg, 65% [based on $Mn_2(CO)_{10}$]. Calc. for $C_{37}H_{32}N_4O_6S_2Mn_2$: C, 55.37; H, 4.02; N, 6.98. Found: C, 54.75; H, 4.03; N, 6.75. IR (CH_2Cl_2, cm^{-1}): $\nu_{(CO)}$ 2025 (m), 2013 (vs), 1927 (s), 1913 (s), $\nu_{(aromatic\ C=C)}$ 1603 (w), $\nu_{(dithiooxamide\ N-C=S)}$ 1494 (w). ^1H NMR (400 MHz, $CDCl_3$): δ 8.30 (d, 2H, H^2, py (nitrogen)), 7.75 (d, 2H, H^2, py (sulfur)), 7.51 (d, 4H, H^2, Ph), 7.40 (t, 4H, H^3, Ph), 7.27 (d, 2H, H^4, Ph), 6.79 (d, 2H, H^3, py (nitrogen)), 6.67 (d, 2H, H^3, py (sulfur)), 4.85 (t, 2H, H^1, CH_2-dithiooxamidato), 3.96 (t, 2H, $H^{1\prime}$, CH_2-dithiooxamidato), 3.34 (t, 2H, H^2, CH_2-dithiooxamidato), 3.17 (t, 2H, $H^{2\prime}$, CH_2-dithiooxamidato), 2.74 (s, 4H, H^1, CH_2-bpp), 2.25 (s, 2H, H^2, CH^2-bpp), ppm. ^{13}C NMR (100 MHz, $CDCl_3$): δ = 194.5 (thioamide CS), 193.1, 192.2, 190.9 [$Mn(CO)_3$], 154.9 (C^2, py, nitrogen), 152.8 (C^4, py, nitrogen), 151.9 (C^2, py, sulfur), 150.8 (C^4, py, sulfur), 139.4, 129.8, 126.6 (Ph, aromatic), 125.6 (C^3, py, nitrogen), 124.2 (C^3, py, sulfur), 62.9, 35.8 (phenethyl), 33.6, 27.3 (methylene) ppm. UV-Vis ($\lambda_{max}{}^{ab}$ (CH_2Cl_2) nm): 232, 302 (LIG), 437 (MLCT) nm. HRMS (ESI): Calcd. For $C_{37}H_{32}N_4O_6S_2Mn_2$ $[M + H]^+$ 803.0603.; found 803.0618.

Single-crystal X-ray diffraction studies

Single-crystal X-ray diffraction data were recorded for the crystals of **4** on a Bruker D8 VENTURE dual source diffractometer equipped with a PHOTON II detector using Mo Kα (λ = 0.71073 Å) radiation at 100 K with the aid of an Oxford Cryosystem unit. A single crystal, selected using polarized optical microscopy, was picked using a fiber loop and mounted on the goniometer and optically centered. The automatic cell determination routine was employed to collect reflections (at different orientations of the detector) and the Bruker APEX4 (ref. 54) suite was used for determining the unit cell parameters, data collection and integration. Semiempirical absorption correction (multi-scan) based on symmetry-equivalent reflections was performed using the SADABS program.[55] The structures were solved by intrinsic phasing and refined by full matrix least-squares, based on F^2 using SHELXT[56] and SHELXL-2019 (ref. 57) in the program WinGX.[58] An attempt was made to model the largest residual electron density peak located near the CH_2Cl_2 solvent molecule as disorder. The occupancy ratios for the two sites for the disordered CH_2Cl_2 molecule were approximately 90 : 10. Anisotropic refinement cycles resulted in the carbon atom turning non-positive definite and hence, the disorder was not modelled. The positions of all the atoms were obtained by direct methods. The graphics were generated using ORTEP-3 (ref. 59) and Mercury 3.8.[60]

MTT assay to assess the toxicity of the compounds

The HEK-293, MG-63 and MCF-7 cells were procured from the National Centre for Cell Science, India and were cultured in DMEM supplemented with 10% FBS at 37 °C in 5% CO_2 conditions. MTT assays were performed with HEK-293, MG-63 and MCF-7 cells as described previously.[61] The MG-63 cells were in Minimum Essential Medium Eagle (MEM) with 10% fetal bovine serum at 37 °C at 5% CO_2. For the MTT assay, the cells were seeded at density of 10 000 cells per well into 96 well cell culture plates (tissue culture grade, 96 wells, flat bottom).[62] After 20 h, old media were discarded and replenished with fresh media (200 μL) in each well. The compounds **2** and **4** were added at the indicated concentrations and incubated for 48 h at 37 °C at 5% CO_2. After 48 h of incubation, the old media were discarded and 100 μL of MTT solution (DMEM medium with MTT at the concentration of 0.5 mg mL^{-1}) to each well of the 96-well plate, followed by the incubation of 3 h period at 37 °C at 5% CO_2. The resultant formazan crystals were dissolved in DMSO and finally, solutions were read by a plate reader at λ_{max} 595 nm. The cell viability percentage is determined by

calculating the ratio of OD value of test cells, which were treated with the indicated compounds to OD value of the control cells, which were treated with DMSO. The values in the graph represent the mean of three independent replicates and the error bars represent the standard deviations. The IC_{50} values were derived from these data by calculating the concentration of the compound required to inhibit the cell viability by 50%. The standard deviations of the IC_{50} values are provided in Table 3.

In silico molecular docking studies

The molecular structure of compound **4**, obtained from single-crystal X-ray diffraction analysis, was used as the ligand for docking simulations.[63] Protein crystal structures of the biological targets epidermal growth factor receptor tyrosine kinase (PDB ID: 1M17) and human matrix metalloproteinase-9 (PDB ID: 1L6J) were retrieved from the RCSB Protein Data Bank (https://www.rcsb.org).[64] Prior to docking, protein structures were prepared by removing water molecules and supplementing missing hydrogens, residues, and partial charges.[65–68] The cavity guided blind molecular docking studies were performed using the AutoDock Vina-based CB-Dock2 web server (https://cadd.labshare.cn/cb-dock2/), which integrates cavity detection and AutoDock Vina-based docking. The results were visualized using PyMOL and Discovery Studio Visualizer v25.1.0.24284 (BIOVIA, San Diego, CA, USA).

Author contributions

Devangana Das: writing – original draft, methodology, investigation, data curation, conceptualization. Nivas Saravanan: writing – review & editing, methodology, formal analysis. Abhishek Kumar: methodology, data curation. Shobhana Krishnaswamy: writing – review & editing, formal analysis, data curation. Arunkumar Dhayalan: writing – review & editing, validation, supervision. Bala. Manimaran: writing – review & editing, validation, supervision, project administration, funding acquisition, conceptualization.

Conflicts of interest

There are no conflicts to declare.

Data availability

CCDC 2471972 (**4**) contains the supplementary crystallographic data for this paper.[69]

The data supporting this article have been included as part of the supplementary information (SI). Supplementary information: stacked IR, overlaid UV-Vis, ^{1}H NMR spectra and ESI-MS isotopic distribution patterns of the compounds **1–4**, docking poses & crystallographic packing diagram of compound **4**. See DOI: https://doi.org/10.1039/d6ra00337k.

Acknowledgements

We thank the SERB-ANRF (Ref no: CRG/2023/000774), Government of India, for financial support. D.D. gratefully acknowledges the University Grants Commission, Government of India for the Savitribai Jyotirao Single Girl Child fellowship (SJSGC). We are thankful to the Central Instrumentation Facility, Pondicherry University, for providing spectral data. We are also thankful to the DST-FIST program sponsored ESI-Mass spectral facility at the Department of Chemistry, Pondicherry University. We acknowledge the DST-FIST funded SCXRD facility, SAIF, IIT Madras, for X-ray intensity data collection.

References

1 R. Nagarajaprakash, C. Ashok Kumar, S. M. Mobin and B. Manimaran, *Organometallics*, 2015, **34**, 724–730.
2 X. Tang, J. Pang, J. Dong, Y. Liu, X.-H. Bu and Y. Cui, *Angew. Chem., Int. Ed.*, 2024, **63**, e202406956.
3 T. R. Cook, V. Vajpayee, M. H. Lee, P. J. Stang and K. W. Chi, *Acc. Chem. Res.*, 2013, **46**, 2464–2474.
4 J. Malberg, M. Bodensteiner, D. Paul, T. Wiegand, H. Eckert and R. Wolf, *Angew. Chem., Int. Ed.*, 2014, **53**, 2771–2775.
5 Y. Tanaka, K. M. C. Wong and V. W. W. Yam, *Angew. Chem., Int. Ed.*, 2013, **52**, 14117–14120.
6 B. Ramakrishna, D. Divya, P. V. Monisha and B. Manimaran, *Eur. J. Inorg. Chem.*, 2015, 5839–5846.
7 M. Sathiyendiran, J. Y. Wu, M. Velayudham, G. H. Lee, S. M. Peng and K. L. Lu, *Chem. Commun.*, 2009, 3795–3797.
8 C. C. Lee, S. C. Hsu, L. L. Lai and K. L. Lu, *Inorg. Chem.*, 2009, **48**, 6329–6331.
9 B. Ramakrishna, R. Nagarajaprakash, V. Veena, N. Sakthivel and B. Manimaran, *Dalton Trans.*, 2015, **44**, 17629–17638.
10 B. Shankar, R. Arumugam, P. Elumalai and M. Sathiyendiran, *ACS Omega*, 2016, **1**(4), 507–517.
11 M. M. Jones and H. R. Clark, *J. Inorg. Nucl. Chem.*, 1971, **33**, 413–419.
12 V. R. Naina, F. Krätzschmer and P. W. Roesky, *Chem. Commun.*, 2022, **58**, 5332–5346.
13 H. Xu, D. C. Xu and Y. Wang, *ACS Omega*, 2017, **10**, 7185–7193.
14 R. D. Hancock and A. Martell, *J. Chem.*, 1996, **73**, 654.
15 R. G. Pearson, *J. Chem. Educ.*, 1968, **45**, 581–587.
16 J. L. Reed, *J. Phys. Chem. A*, 2012, **116**, 7147–7153.
17 J. L. Reed, *Inorg. Chem.*, 2008, **47**, 5591–5600.
18 R. G. Pearson, *J. Am. Chem. Soc.*, 1963, **85**, 3533–3539.
19 K. L. Haas and K. J. Franz, *Chem. Rev.*, 2009, **109**, 4921–4960.
20 J. L. Hovey, T. M. Dittrich and M. J. Allen, *J. Rare Earths*, 2023, **41**, 1–18.
21 A. M. Hamisu, A. Ariffin and A. C. Wibowo, *Inorg. Chim. Acta*, 2020, **511**, 119801.
22 B. Askari, H. A. Rudbari, N. Micale, T. Schirmeister, T. Efferth, E. Jeong Seo, G. Bruno and K. Schwickertc, *Dalton Trans.*, 2019, **48**, 15869–15887.
23 M. C. Aversa, P. Bonaccorsi, D. W. Bruce, F. Caruso, P. Giannetto, S. Lanza and S. Morrone, *Inorg. Chim. Acta*, 1997, **256**, 235–241.
24 M. Perec, R. Baggio and M. T. Garland, *Acta Crystallogr.*, 1995, **51**, 2182–2184.
25 R. N. Hurd, G. D. L. Mater, G. C. Mcelheny, R. J. Turner and V. H. Wallingford, *J. Org. Chem.*, 1961, **26**, 3980–3987.

26 M. S. Refat, H. K. Ibrahim, S. Z. A. Sowellim, M. H. Soliman, E. M. Saeed and J. Inorg, *Organomet. Polym.*, 2009, **19**, 521–531.
27 S. Nivas, U. Kumar, D. Das, D. Thamarainathan, D. Tripathi, S. Krishnaswamy, R. Padmanaban, N. Sakthivel and B. Manimaran, *J. Mol. Struct.*, 2025, **1342**, 142741.
28 B. Askari, H. A. Rudbari, N. Micale, T. Schirmeister, A. Giannetto, S. Lanza, G. Bruno and V. Mirkhani, *Polyhedron*, 2019, **164**, 195–201.
29 B. Askari, H. A. Rudbari, N. Micale, T. Schirmeister, A. Maugeri and M. Navarra, *J. Organomet. Chem.*, 2019, **900**, 120918.
30 C. L. Kee, F. Zhou, H. Su and Y. K. Yan, *J. Organomet. Chem.*, 2015, **792**, 211–219.
31 C. N. R. Rao and R. Venkataraghavan, *Spectrochim. Acta Part A Mol. Spectrosc.*, 1989, **45**, 299–305.
32 D. Gupta, P. Rajakannu, B. Shankar, R. Shanmugam, F. Hussain, B. Sarkar and M. Sathiyendiran, *Dalton Trans.*, 2011, **40**, 5433–5435.
33 R. Nagarajaprakash, R. Govindarajan and B. Manimaran, *Dalton Trans.*, 2015, **44**, 11732–11740.
34 R. Nagarajaprakash, D. Divya, B. Ramakrishna and B. Manimaran, *Organometallics*, 2014, **33**, 1367–1373.
35 M. Mazloum-Ardakani, B. Barazesh, S. M. Moshtaghioun and M. H. Sheikhha, *Sci. Rep.*, 2019, **9**, 14966.
36 M. Ghasemi, T. Turnbull, S. Sebastian and I. Kempson, *Int. J. Mol. Sci.*, 2021, **22**, 12827.
37 M. Azam, S. I. Al-Resayes, A. Trzesowska-Kruszynska, R. Kruszynski, A. Verma and U. K. Pati, *Inorg. Chem. Commun.*, 2014, **46**, 73–80.
38 R. K. Singh, S. Awasthi, A. Dhayalan, J. M. F. Ferreira and S. Kannan, *Mater. Sci. Eng., C*, 2016, **62**, 692–701.
39 R. K. Singh, M. Srivastava, N. K. Prasad, S. Awasthi, A. Dhayalan and S. Kannan, *Mater. Sci. Eng., C*, 2017, **78**, 715–726.
40 C. Ashok Kumar, R. Nagarajaprakash, W. Victoria, V. Veena, N. Sakthivel and B. Manimaran, *Inorg. Chem. Commun.*, 2016, **64**, 39–44.
41 A. S. Martins, A. L. M. Batista de Carvalho, I. Lamego, M. P. M. Marques and A. M. Gil, *ChemistrySelect*, 2020, **5**, 5993–6000.
42 D. Divya, R. Nagarajaprakash, P. Vidhyapriya, N. Sakthivel and B. Manimaran, *ACS Omega*, 2019, **4**, 12790–12802.
43 A. Anil, D. Tripathi, S. Shankar, S. S. Nayak, R. Krishna, U. Kumar, B. Manimaran and N. Sakthivel, *Spectrochim. Acta, Part A Mol. Biomol. Spectrosc.*, 2026, **350**, 127406.
44 A. A. Magray, J. Varghese, N. Saravanan, G. Gupta, C. Y. Lee, S. Yeswanth Kumar, R. Padmanaban, D. Tripathi, N. Sakthivel and B. Manimaran, *Inorg. Chem.*, 2025, **64**, 13941–13955.
45 G. Tamasi, A. Merlino, F. Scaletti, P. Heffeter, A. A. Legin, M. A. Jakupec, W. Berger, L. Messori, B. K. Keppler and R. Cini, *Dalton Trans.*, 2017, **46**, 3025–3040.
46 J. Stamos, M. X. Sliwkowski and C. Eigenbrot, *J. Biol. Chem.*, 2002, **277**, 46265–46272.
47 P. A. Elkins, Y. S. Ho, W. W. Smith, C. A. Janson, K. J. D'Alessio, M. S. McQueney, M. D. Cummings and A. M. Romanic, *Acta Crystallogr., Sect. D: Biol. Crystallogr.*, 2002, **58**, 1182–1192.
48 M. G. Salem, S. A. Abu El-ata, E. H. Elsayed, S. N. Mali, H. A. Alshwyeh, G. Almaimani, R. A. Almaimani, H. A. Almasmoum, N. Altwaijry, E. Al-Olayan, E. M. Saied and M. F. Youssef, *RSC Adv.*, 2023, **13**, 33080–33095.
49 O. Trott and A. J. Olson, *J. Comput. Chem.*, 2010, **31**, 455–461.
50 X. Yang, Y. Liu, J. Gan, Z.-X. Xiao and Y. Cao, *Brief. Bioinform.*, 2022, **23**, 1–11.
51 Y. Liu, X. Yang, J. Gan, S. Chen, Z.-X. Xiao and Y. Cao, *Nucleic Acids Res.*, 2022, **50**, W159–W164.
52 A. Giannetto, F. Puntoriero, A. Barattucci, S. Lanza and S. Campagna, *Inorg. Chem.*, 2009, **48**, 10397–10404.
53 W. L. F. Armarego and C. L. L. Chai, *Purification of Laboratory Chemicals*, Butterworth-Heinemann, Elseiver Inc, Oxford, 6th edn, 2009.
54 Bruker, *Apex4 Suite – APEX4, SAINT and SADABS*, Bruker AXS Inc., 2021, Madison, Wisconsin, USA.
55 L. Krause, R. Herbst-Irmer, G. M. Sheldrick and D. Stalke, *J. Appl. Cryst.*, 2015, **48**, 3–10.
56 G. M. Sheldrick, *Acta Crystallogr., Sect. A*, 2015, **71**, 3–8.
57 G. M. Sheldrick, *Acta Crystallogr., Sect. C*, 2015, **71**, 3–8.
58 L. J. Farrugia, *J. Appl. Crystallogr.*, 2012, **45**, 849–854.
59 ORTEP-3 for Windows: L. J. Farrugia, *J. Appl. Cryst.*, 1997, **30**, 568.
60 C. F. Macrae, I. J. Bruno, J. A. Chisholm, P. R. Edgington, P. McCabe, E. Pidcock, L. Rodriguez-Monge, R. Taylor, J. van de Streek and P. A. Wood, *J. Appl. Cryst.*, 2008, **41**, 466–470.
61 E. S. Al-Sheddi, M. M. Al-Oqail, Q. Saquib, M. A. Siddiqui, J. Musarrat, A. Ali Al-Khedhairy and N. N. Farshori, *Molecules*, 2015, **20**, 8181–8197.
62 A. Alzamami, E. M. Radwan, E. Abo-Elabass, M. El Behery, H. A. Alshwyeh, E. Al-Olayan, A. S. Altamimi, N. G. M. Attallah, N. Altwaijry, M. Jaremko and E. M. Saied, *BMC Chem.*, 2023, **17**, 174.
63 V. L. Maruthanila, R. Elancheran, V. L. Chandraboss, S. Kabilan and S. Mirunalini, *J. Mol. Struct.*, 2024, **1318**, 139131.
64 H. M. Berman, J. Westbrook, Z. Feng, G. Gilliland, T. N. Bhat, H. Weissig, I. N. Shindyalov and P. E. Bourne, *Nucleic Acids Res.*, 2000, **28**, 235–242.
65 E. V. Panova, J. K. Voronina and D. A. Safin, *Inorg. Chem. Commun.*, 2024, **166**, 112407.
66 S. Adhikari, S. Nath, S. Kansız, N. Balidya, A. K. Paul, N. Dege, O. Sahin, G. Mahmoudi, A. K. Verma and D. A. Safin, *J. Inorg. Biochem.*, 2024, **257**, 112598.
67 E. V. Panova, J. K. Voronina, A. N. Azizova, Ö. F. Tutar, G. Mahmoudi and D. A. Safin, *J. Mol. Struct.*, 2026, **1352**, 144040.
68 S. M. Khirallah, H. M. M. Ramadan, H. A. A. Aladl, N. O. Ayaz, L. A. F. Kurdi, M. Jaremko, S. Z. Alshawwa and E. M. Saied, *Pharmaceuticals*, 2022, **15**, 1576.
69 CCDC 2471972: Experimental Crystal Structure Determination, 2026, DOI: 10.5517/ccdc.csd.cc2nz910.